nature biotechnology

Potentiating antibacterial activity by predictably enhancing endogenous microbial ROS production

Mark P Brynildsen[1,5,6], Jonathan A Winkler[1,2,6], Catherine S Spina[1,3,4], I Cody MacDonald[1] & James J Collins[1–4]

The ever-increasing incidence of antibiotic-resistant infections combined with a weak pipeline of new antibiotics has created a global public health crisis[1]. Accordingly, novel strategies for enhancing our antibiotic arsenal are needed. As antibiotics kill bacteria in part by inducing reactive oxygen species (ROS)[2–4], we reasoned that targeting microbial ROS production might potentiate antibiotic activity. Here we show that ROS production can be predictably enhanced in *Escherichia coli*, increasing the bacteria's susceptibility to oxidative attack. We developed an ensemble approach of genome-scale, metabolic models capable of predicting ROS production in *E. coli*. The metabolic network was systematically perturbed and its flux distribution analyzed to identify targets predicted to increase ROS production. Targets that were predicted *in silico* were experimentally validated and further shown to confer increased susceptibility to oxidants. Validated targets also increased susceptibility to killing by antibiotics. This work establishes a systems-based method to tune ROS production in bacteria and demonstrates that increased microbial ROS production can potentiate killing by oxidants and antibiotics.

Reactive oxygen species (ROS) can damage DNA, RNA, proteins and lipids, resulting in cell death when the level of ROS exceeds an organism's detoxification and repair capabilities. Despite this danger, bacteria growing aerobically generate ROS as a metabolic by-product, a risk balanced by an increased efficiency and yield of energy from growth substrates. At least two possible mechanisms can be used to manipulate bacterial ROS metabolism and increase sensitivity of bacteria to oxidative attack: (i) amplification of endogenous ROS production and (ii) impairment of detoxification and repair systems. Whereas removal of their detoxification and repair systems has been shown to make bacteria more susceptible to oxidants[5,6], antibiotics[7] and immune attack[8,9], manipulation of endogenous bacterial ROS production remains largely unexplored. Endogenous ROS production has long been appreciated as a factor influencing the ability of an organism to survive oxidative stress[10], but an inability to predict the outcome of genetic and environmental perturbations on ROS production[11] has hampered exploration of this phenomenon as an antimicrobial adjuvant. What has been missing is a thorough systems-level understanding of the pathways that produce ROS, which constitute a potentially expansive and highly integrated biochemical reaction network. In this study, we sought to tune *E. coli* metabolism for increased ROS production (specifically, O_2^- and H_2O_2) and to determine whether this effect can potentiate oxidative stress and antibiotic activity. Our goal was not to overwhelm the oxidative detoxification and repair capabilities of *E. coli* with endogenously generated ROS, but rather to increase endogenous production such that the ability of *E. coli* to cope with exogenous oxidative stress would be compromised. We hypothesized that such a strategy would broadly potentiate antimicrobials that harness oxidative stress and provide a general approach for the discovery of antimicrobial adjuvants. To reach this goal, we developed an approach using ensembles of genome-scale, metabolic models to quantitatively estimate ROS production from *E. coli* metabolism (**Fig. 1**).

The sources for the majority of endogenous ROS produced by *E. coli* remain elusive[11]. The removal of enzymes that generate ROS *in vitro* has had seemingly little effect on whole-cell ROS production[11]. This can be explained by the potential scope of ROS generators. Previous studies have demonstrated that O_2^- and H_2O_2 can be produced when O_2 abstracts electrons from reduced flavin, quinol and transition metal functional groups[12,13]. We inspected *E. coli* metabolism for enzymes that use these electron carriers and identified 133 reactions, spanning many metabolic pathways, with the potential to generate ROS in the presence of O_2 (**Supplementary Table 1**). The number of potential ROS-generating reactions is comparable to the number of reactions that generate ATP/ADP, NAD/H and NADP/H, suggesting that ROS could play a crucial, highly integrated role in bacterial metabolism. A quantitative systems-level approach is required to predictably modify the production of such highly connected metabolites, as even removal of enzymes that endogenously produce ROS may increase or decrease production depending on the redistribution of metabolic flux on the remaining ROS-generating enzymes[11].

Systems-level metabolic modeling has been used extensively to optimize the production of desirable metabolites and has led to advances in biotechnology, metabolic discovery and microbiology[14]. In this study, we employed flux balance analysis with genome-scale

[1]Howard Hughes Medical Institute, Department of Biomedical Engineering, and Center for BioDynamics, Boston University, Boston, Massachusetts, USA. [2]Program in Molecular Biology, Cell Biology, and Biochemistry, Boston University, Boston, Massachusetts, USA. [3]Boston University School of Medicine, Boston, Massachusetts, USA. [4]Wyss Institute for Biologically Inspired Engineering, Harvard University, Boston, Massachusetts, USA. [5]Present address: Department of Chemical and Biological Engineering, Princeton University, Princeton, New Jersey, USA. [6]These authors contributed equally to this work. Correspondence should be addressed to J.J.C.(jcollins@bu.edu).

Received 8 June 2012; accepted 20 November 2012; published online 6 January 2013; doi:10.1038/nbt.2458

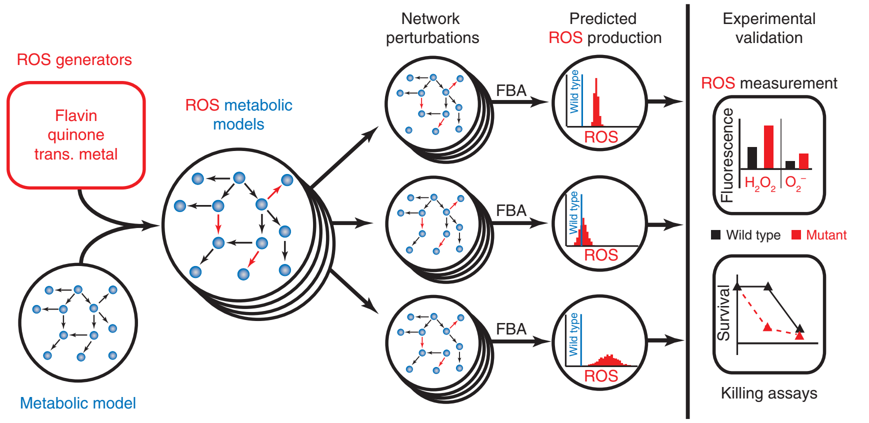

Figure 1 Systems approach to enhance microbial ROS production. Left, methodology for the development and validation of an ensemble of systems-level models of *E. coli* metabolism for estimation of basal ROS production. ROS-generating reactions were incorporated into a metabolic reconstruction and flux balance analysis (FBA) framework[17]. Network perturbations by single-gene knockouts were done *in silico* using FBA to identify alterations that affect ROS production. Right, *in silico* predictions were evaluated experimentally by generating mutants and measuring their ROS production and susceptibility to killing by oxidants and antibiotics. Trans., transition.

metabolic models (GSMM) to simulate systems-level ROS production in *E. coli*. In flux balance analysis, reaction stoichiometries are used to place constraints on a metabolic solution space, and linear programming identifies a flux distribution within that space that optimizes an objective function, which is typically a flux within the system, such as biomass generation. Accuracy within the stoichiometric reaction network is critical to the performance of such constraint-based techniques[15,16]. Current metabolic reconstructions include consumption reactions, such as superoxide dismutase and catalase, and generation reactions involved in cofactor biosynthesis and alternate carbon metabolism, but are devoid of generation reactions that account for the majority of ROS produced[17] (**Supplementary Table 2**). To construct a metabolic model capable of estimating ROS production, we added 266 additional ROS production reactions to the *E. coli* GSMM[17], one O_2^-- and one H_2O_2-producing reaction for each of the 133 potential sources (Online Methods, **Supplementary Methods** and **Supplementary Table 1**). These potential ROS sources included all enzymes known to generate H_2O_2 and O_2^- in *E. coli*[11,13,17,18], and this framework allowed separate (independent species balances), but simultaneous, modeling of H_2O_2 and O_2^- production in *E. coli*.

Optimization of an objective function is a critical feature of constraint-based techniques, and maximizing for biomass generation has proven to be effective in predicting redistribution of metabolic flux[19]. However, when presented with competing pathways, constraint-based methods will identify the most efficient pathway in terms of cellular resources as the one that carries flux. ROS-generating reactions are less efficient competing pathways where reducing equivalents are lost to O_2 instead of being transferred to the intended acceptor. Therefore, addition of ROS-generating reactions to a GSMM is necessary to model ROS metabolism, but insufficient because the reactions will not carry flux (**Supplementary Methods**). To address this, we recognized that ROS-generating reactions are coupled to their more efficient counterpart, in the sense that initial electron transfer from reactant to electron carrier proceeds normally and is dictated by requirements for the intended products, and that it is the promiscuity of the reduced electron carrier with O_2 that generates ROS. Thus, ROS flux is a function of the number of electrons transferred to the electron carrier, and consequently dependent on the reaction flux of the intended reaction. Therefore, in this study, the flux of O_2^- and H_2O_2 from ROS-generating enzyme$_i$ was assumed to be proportional to the reaction flux, v_i. This assumption results in proportionality between ROS flux from enzyme$_i$ and the number of electrons transferred by enzyme$_i$, and is accomplished by coupling the intended enzyme reaction to both its O_2^- and H_2O_2 side reactions (Online Methods and **Supplementary Methods**). This coupling requires specification of the proportion of electrons that flow to O_2 to form O_2^- and H_2O_2 for each of the 133 potential ROS sources. These values vary considerably from enzyme to enzyme[12,20], and are largely undefined owing to the absence of *in vivo* measurements. With this indeterminacy in mind, we employed an approach using ensembles of models.

Two ensembles of ROS-GSMMs were constructed, each with 1,000 different models (**Supplementary Methods**). The proportions of electron flow from reaction$_i$ to generate O_2^- and H_2O_2 were captured by the constants c_{i,O_2^-} and c_{i,H_2O_2} (**Supplementary Methods** and **Supplementary Dataset**). One ensemble derived these constants from a Gaussian distribution to model a distributed ROS production network (many significant generators), whereas the other ensemble derived these constants from an exponential distribution to model a centralized ROS production network (few significant generators). Further, it was specified that ROS could only be produced from these reactions and not consumed, with the exception of the O_2^- attack of Fe-S centers, and that the *in silico* O_2^- and H_2O_2 production rates of the wild-type GSMM had to match the best available experimental estimates (Online Methods and **Supplementary Methods**). Thus, every stoichiometric reaction network within the ensembles had the exact same production rate of O_2^- and H_2O_2 for its wild-type GSMM. Also, the existence of alternative optimal solutions for ROS production of each wild-type network was examined using flux variability analysis. At a biomass production rate of 100%, all wild-type networks generate a unique solution for the flux of H_2O_2 and O_2^- (**Supplementary Methods**).

With these ensembles, we explored *in silico* how perturbations to the metabolic network alter basal ROS production. We performed a systematic gene-deletion analysis in which we removed genes one at a time and recalculated reaction fluxes, while optimizing for biomass generation (Online Methods and **Supplementary Methods**). This provided quantitative distributions of ROS production (H_2O_2 and O_2^-) from mutant *E. coli* (**Fig. 1**) and allowed us to identify deletions likely to alter basal ROS production, as measured by the mean ROS production level (**Fig. 2a,b** and **Supplementary Fig. 1a**). To account for variable growth rates of mutant strains, we normalized ROS flux by biomass production (BM), and calculations are therefore H_2O_2/BM and O_2^-/BM (mmol/g dry weight (DW) produced). From our analysis of bacteria grown in aerobic glucose minimal media (see **Supplementary Table 3** for constraints imposed by transcriptional regulation), we identified genes whose deletions were most likely to increase ROS production, including those encoding for ATP synthase (*atpA-I*), pyruvate dehydrogenase (*aceEF, lpd*), NADH dehydrogenase complex I (*nuoABCE-N*), glutamate dehydrogenase (*gdhA*), cytochrome *bo* (*cyoABCD*) and triose phosphate isomerase (*tpiA*)

(**Supplementary Table 4**). Investigation of the flux distributions for these mutants identified a general trend for ROS production where predicted increases correlated with inefficiencies in the production or usage of ATP.

To validate our approach and *in silico* analysis, we experimentally tested a series of deletions of genes that encode enzymes within glycolysis, the pentose-phosphate pathway, the Entner-Doudoroff pathway, the TCA cycle, the glyoxylate shunt, aerobic respiration, acetate metabolism and glutamate metabolism (**Fig. 2c,d** and **Supplementary Fig. 1b**). This collection of enzymes included those predicted to increase ROS (targets) as well as those predicted to leave ROS production unchanged (negative controls). We note that our predictions included all 21 genetic mutants tested, both targets and negative controls, and that only those enzymes that were experimentally tested are

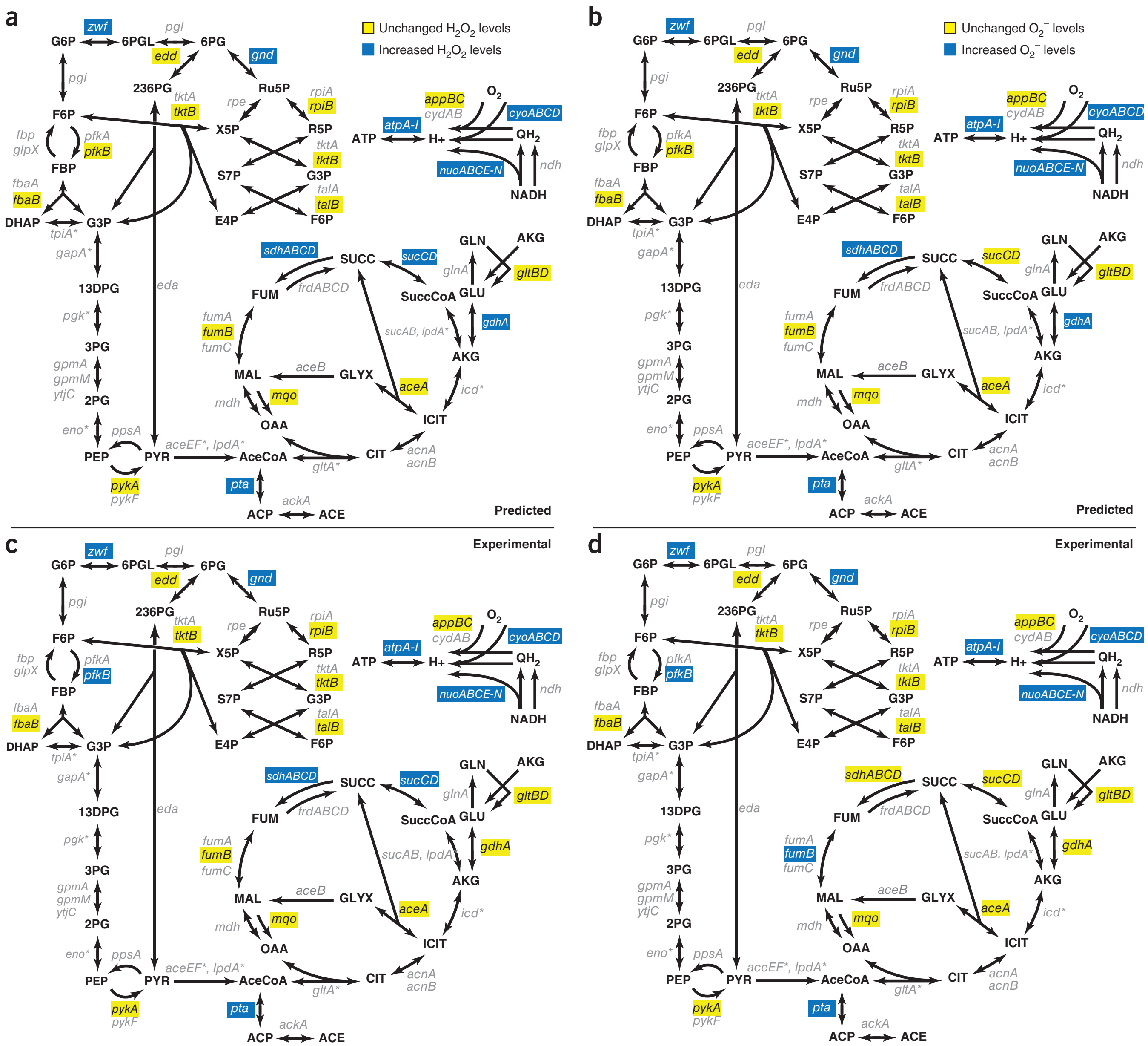

Figure 2 *In silico* predictions and experimental measures of H_2O_2 and O_2^- levels. (**a**) Predicted H_2O_2 levels of various mutants compared to wild type. Blue, strains whose mean H_2O_2 production levels were simulated to be >5% higher than wild type over both ensembles; yellow, strains whose mean H_2O_2 production levels were simulated to be <5% higher. (**b**) Predicted O_2^- levels of various mutants compared to wild type. Blue, strains whose mean O_2^- production levels were simulated to be >5% higher than wild type over both ensembles; yellow, strains whose mean O_2^- production levels were simulated to be <5% higher. (**c**) Experimentally measured relative fluorescence/A_{600} of strains with the H_2O_2-sensitive reporter (*dps* promoter-gfp). Blue, strains that were experimentally measured to have higher levels of H_2O_2 compared with wild type ($P < 0.05$); yellow, strains that were experimentally measured to have levels of H_2O_2 that do not exceed those of wild type. (**d**) Experimentally measured relative fluorescence/A_{600} of strains with the O_2^--sensitive reporter (*soxS* promoter-gfp). Blue, strains that were experimentally measured to have increased levels of O_2^- compared with wild type ($P < 0.05$); yellow, strains that were experimentally measured to have levels of O_2^- that do not exceed those of wild type. * denotes genes that are essential in our media conditions. Gray denotes genes that were not experimentally examined (for consistency between diagrams, these genes were also denoted by gray in **a** and **b**, although *in silico* predictions were computed).

Figure 3 Evaluation of susceptibility to killing by oxidants. (**a**–**c**) Time course of predicted target strains and wild type treated with H_2O_2 (**a**), menadione (**b**) and NaOCl (**c**). (**d**–**f**) Time course of negative control strains and wild type treated with H_2O_2 (**d**), menadione (**e**) and NaOCl (**f**). Error bars, mean ± s.e.m. for all plots.

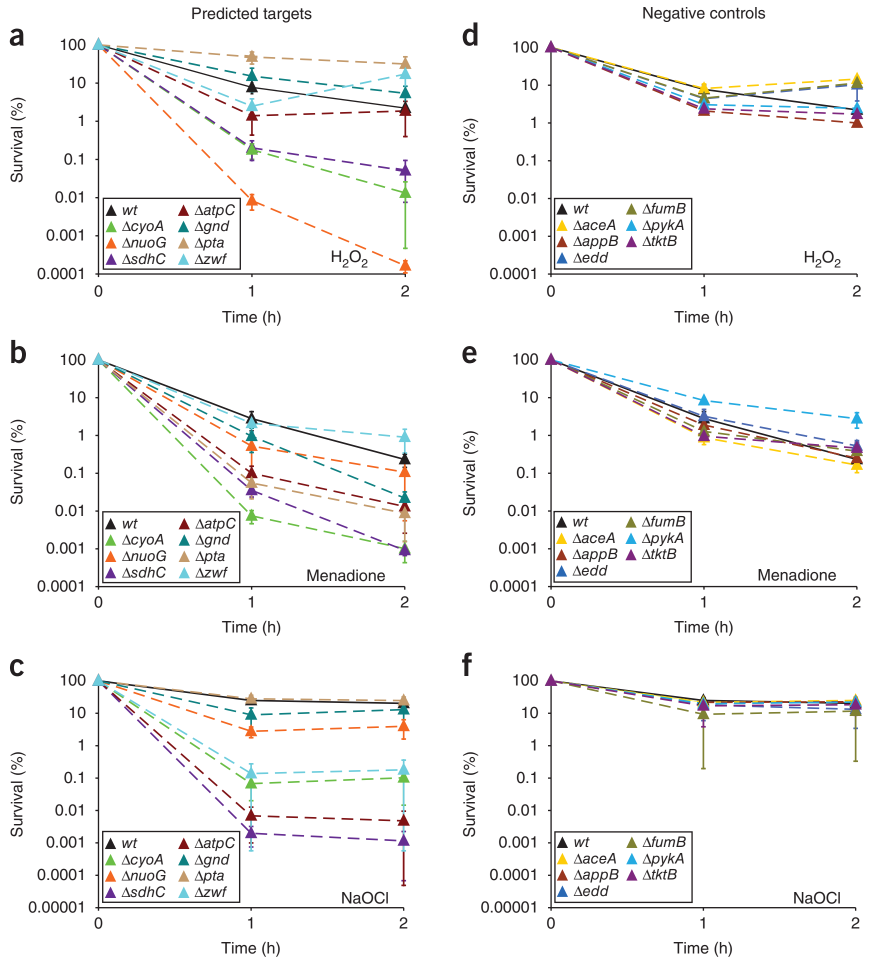

color-coded in **Figure 2** and **Supplementary Figure 1**. We selected isozymes for testing on the basis of literature evidence that suggested their removal would most closely reflect model assumptions, and we did not test deletions of pyruvate dehydrogenase and triose-phosphate isomerase because they did not grow in minimal glucose media (**Supplementary Methods**).

To measure O_2^-, we used a SoxR-controlled GFP-reporter system, whereas to measure H_2O_2, we used both an OxyR-controlled GFP-reporter system and the direct-sensing HyPer protein (Online Methods). Our experimental results showed 80–90% qualitative agreement with our *in silico* predictions of H_2O_2 and O_2^- production (**Fig. 2** and **Supplementary Fig. 1**; correct predictions: *dps*-GFP: 19/21, *soxS*-GFP: 17/21, HyPer: 17/21). The probabilities that these levels of agreement would have occurred by chance, using the null hypothesis that random segregation of the 21 genes into targets and negative controls would match experimental results as well as predictions from our modeling approach, are 3.7×10^{-4} (*dps*-GFP), 1.0×10^{-2} (*soxS*-GFP) and 6.2×10^{-3} (HyPer) (Online Methods). These experimental results suggest that our systems-level approach using model ensembles enables predictable tuning of ROS production in *E. coli*.

We next asked if increased basal production of O_2^- and/or H_2O_2 would make such strains more susceptible to killing by oxidants. We tested the oxidants O_2^- (generated via menadione) and H_2O_2 because of their inclusion in the model and importance for antibiotic action[3]; we chose NaOCl (bleach) because it is used as a biocide. Strains chosen for testing of oxidant sensitivity were those with *in silico* predictions of increased production (targets) or unchanged production (negative controls) that was confirmed by experimental results (**Fig. 2**). Our results indicate that increased basal production of O_2^- or H_2O_2 generally increases microbial susceptibility to oxidative attack (**Fig. 3**). Strains with genetic deletions that increase ROS production were more susceptible to oxidants, whereas the negative-control strains, which had wild-type production levels of ROS, did not. The probability this enrichment would have been observed by random selection is 2.5×10^{-5} and demonstrates that increased production of O_2^- and H_2O_2 can potentiate killing by oxidants. We note that some mutant strains predicted to increase ROS production conferred increased susceptibility to all oxidants tested (*ΔcyoA* and *ΔsdhC*), whereas others showed selective increases in sensitivity (e.g., *Δzwf*), suggesting that sensitivity to one oxidant does not always translate to other oxidants. This is not surprising, and likely derives from the differences in biochemical activity of the oxidants and the distinct cellular-death pathways they induce[20,21]. Our results clearly demonstrate that increasing endogenous production is a robust strategy to enhance the susceptibility of microbes to oxidative stress.

Bactericidal antibiotics have been shown to share a common mechanism of cell death that involves the production of ROS[3]. We investigated whether increased basal production of ROS could potentiate the action of bactericidal antibiotics (the β-lactam ampicillin, the fluoroquinolones ofloxacin and ciprofloxacin, and the aminoglycoside gentamicin) (**Fig. 4**). Three of the validated targets (*ΔcyoA*, *ΔnuoG*, *ΔsdhC*) had increased sensitivity to both β-lactam and fluoroquinolone antibiotics (**Fig. 4a**,**b** and **Supplementary Fig. 2a**) and one of the targets (*Δpta*) exhibited increased sensitivity to only fluoroquinolones (**Fig. 4b** and **Supplementary Fig. 2a**), whereas all of the negative-control strains displayed wild-type sensitivity to both antibiotic classes (**Fig. 4c**,**d** and **Supplementary Fig. 2b**). Our approach therefore correctly predicted strain sensitivity to both β-lactams and fluoroquinolone antibiotics over 70% of the time. We also tested sensitivity to aminoglycosides, though we reasoned that increased killing, in general, would not be observed. This expectation was based on the fact that many of the gene deletions that increase basal ROS production negatively affect proton motive force, which is important for aminoglycoside uptake[22]. As expected, the negative controls had similar sensitivity to gentamicin as wild type, whereas many targets had decreased sensitivity (**Supplementary Fig. 2c**,**d**). We note that *ΔatpC* had increased sensitivity toward gentamicin, which we believe may be the result of its positive impact on proton motive force[23] as well as its effect on basal ROS production. These data indicate that bactericidal antibiotic primary target

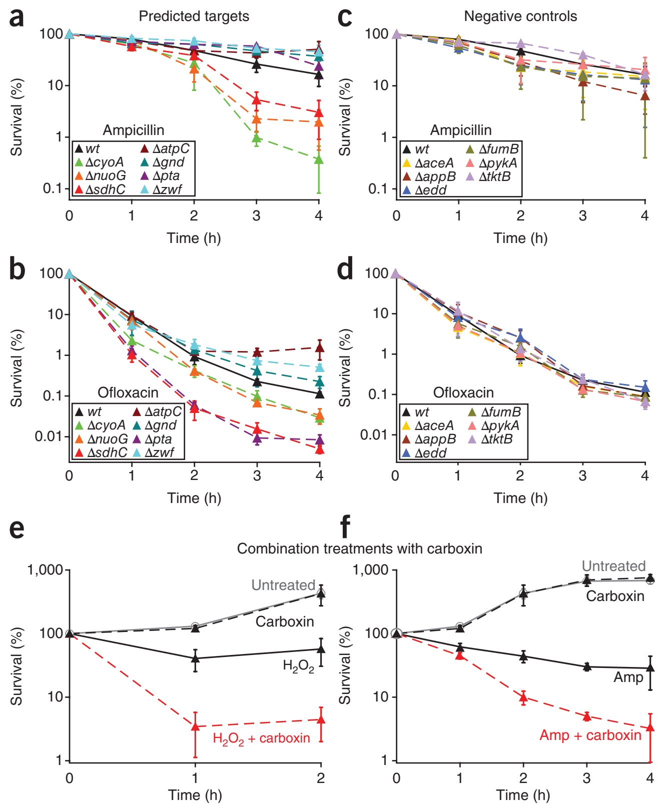

Figure 4 Evaluation of susceptibility to killing by bactericidal antibiotics and combination treatments with a chemical inhibitor. (**a**,**b**) Time course of predicted target strains and wild type treated with ampicillin (**a**) and ofloxacin (**b**). (**c**,**d**) Time course of negative control strains and wild type treated with ampicillin (**c**) and ofloxacin (**d**). (**e**) Time course of wild-type cells treated with carboxin alone, H_2O_2 alone, a combination of carboxin and H_2O_2, or no treatment. (**f**) Time course of wild-type cells treated with carboxin alone, ampicillin alone, a combination of carboxin and ampicillin, or no treatment. Error bars, mean ± s.e.m. for all plots.

interactions must be enabled (e.g., by antibiotic uptake) to leverage ROS production as an adjuvant therapy. Accordingly, we expected and demonstrated that the activities of bacteriostatic antibiotics, which do not produce ROS[6], are unaffected by increases in basal ROS production (**Supplementary Fig. 3**).

We also asked whether chemical inhibition of one of the validated targets could increase sensitivity to oxidants and bactericidal antibiotic treatment. We treated wild type with carboxin, an inhibitor of succinate dehydrogenase, and measured susceptibility toward H_2O_2 and ampicillin, respectively. Addition of carboxin alone had no effect on the growth of wild-type cells (**Fig. 4e**,**f**). However, wild-type cells treated with H_2O_2 and carboxin demonstrated increased sensitivity compared to wild-type cells treated with H_2O_2 alone (**Fig. 4e**). Similarly, wild-type cells treated with ampicillin and carboxin were more sensitive to the antibiotic than cells treated with ampicillin alone (**Fig. 4f**). To more fully examine this synergy, we conducted a systematic drug screen spanning five concentrations for each compound (carboxin and ampicillin) including the untreated sample. This allowed us to calculate that carboxin concentrations of 250 μM or greater are synergistic with ampicillin concentrations of 7.5–10 μg/ml, using the Bliss Independence and Highest Single Agent models of drug synergism (**Supplementary Fig. 4**). These results show that chemical inhibition of a predicted and validated target (succinate dehydrogenase) is sufficient to increase sensitivity to oxidative attack and antibiotic treatment. Although carboxin may not be suitable as an antibiotic adjuvant due to toxicity concerns (http://www.epa.gov/oppsrrd1/REDs/factsheets/0012fact_carboxin.pdf), validation that chemical inhibition of succinate dehydrogenase confers sensitivity similar to that of genetic perturbation opens the possibility of using chemical library screening to find nontoxic inhibitors of bacterial succinate dehydrogenase and other predicted targets. Chemical libraries have been successfully screened for compounds with antimicrobial properties against pathogenic bacteria[24] and our method complements this work by identifying novel enzyme targets for compounds that may have no antimicrobial properties alone, but which enhance the killing efficacy of current antibacterial agents.

Here we established a systems-based method to predictably tune microbial ROS production. By developing genome-scale ROS metabolic models, we were able to predict redistribution of ROS flux resulting from network perturbations and demonstrate experimentally that increased ROS flux can potentiate oxidative attack from antibiotic and biocide treatment. This approach allows rapid identification of antibacterial adjuvant targets and is translatable to other pathogens of interest, such as *Mycobacterium tuberculosis*, *Staphylococcus aureus*, *Haemophilus influenzae* and *Salmonella typhimurium*, for which metabolic reconstructions are available[25–28]. In addition, the increasingly rapid construction of genome-scale metabolic models will extend the breadth of the technique[29], opening up the possibility of using it to target newly identified resistant strains.

METHODS

Methods and any associated references are available in the online version of the paper.

Note: Supplementary information is available in the online version of the paper.

ACKNOWLEDGMENTS

This work was supported by the National Institutes of Health Director's Pioneer Award Program and the Howard Hughes Medical Institute.

AUTHOR CONTRIBUTIONS

M.P.B., J.A.W. and J.J.C. designed the study, analyzed the results and wrote the manuscript. Experiments were done by M.P.B., J.A.W., C.S.S. and I.C.M.

COMPETING FINANCIAL INTERESTS

The authors declare competing financial interests: details are available in the online version of the paper.

Published online at http://www.nature.com/doifinder/10.1038/nbt.2458.
Reprints and permissions information is available online at http://www.nature.com/reprints/index.html.

1. Arias, C.A. & Murray, B.E. Antibiotic-resistant bugs in the 21st century–a clinical super-challenge. *N. Engl. J. Med.* **360**, 439–443 (2009).
2. Foti, J.J., Devadoss, B., Winkler, J.A., Collins, J.J. & Walker, G.C. Oxidation of the guanine nucleotide pool underlies cell death by bactericidal antibiotics. *Science* **336**, 315–319 (2012).
3. Kohanski, M.A., Dwyer, D.J., Hayete, B., Lawrence, C.A. & Collins, J.J. A common mechanism of cellular death induced by bactericidal antibiotics. *Cell* **130**, 797–810 (2007).
4. Kohanski, M.A., Dwyer, D.J., Wierzbowski, J., Cottarel, G. & Collins, J.J. Mistranslation of membrane proteins and two-component system activation trigger antibiotic-mediated cell death. *Cell* **135**, 679–690 (2008).
5. Carlioz, A. & Touati, D. Isolation of superoxide dismutase mutants in *Escherichia coli*: is superoxide dismutase necessary for aerobic life? *EMBO J.* **5**, 623–630 (1986).
6. Loewen, P.C. Isolation of catalase-deficient *Escherichia coli* mutants and genetic mapping of katE, a locus that affects catalase activity. *J. Bacteriol.* **157**, 622–626 (1984).

7. Dwyer, D.J., Kohanski, M.A., Hayete, B. & Collins, J.J. Gyrase inhibitors induce an oxidative damage cellular death pathway in *Escherichia coli*. *Mol. Syst. Biol.* **3**, 91 (2007).
8. Hebrard, M., Viala, J.P., Meresse, S., Barras, F. & Aussel, L. Redundant hydrogen peroxide scavengers contribute to Salmonella virulence and oxidative stress resistance. *J. Bacteriol.* **191**, 4605–4614 (2009).
9. Liu, C.I. *et al.* A cholesterol biosynthesis inhibitor blocks *Staphylococcus aureus* virulence. *Science* **319**, 1391–1394 (2008).
10. Imlay, J.A. & Fridovich, I. Assay of metabolic superoxide production in *Escherichia coli*. *J. Biol. Chem.* **266**, 6957–6965 (1991).
11. Korshunov, S. & Imlay, J.A. Two sources of endogenous hydrogen peroxide in *Escherichia coli*. *Mol. Microbiol.* **75**, 1389–1401 (2010).
12. Massey, V. Activation of molecular oxygen by flavins and flavoproteins. *J. Biol. Chem.* **269**, 22459–22462 (1994).
13. Messner, K.R. & Imlay, J.A. The identification of primary sites of superoxide and hydrogen peroxide formation in the aerobic respiratory chain and sulfite reductase complex of *Escherichia coli*. *J. Biol. Chem.* **274**, 10119–10128 (1999).
14. Feist, A.M. & Palsson, B.O. The growing scope of applications of genome-scale metabolic reconstructions using *Escherichia coli*. *Nat. Biotechnol.* **26**, 659–667 (2008).
15. Becker, S.A. & Palsson, B.O. Context-specific metabolic networks are consistent with experiments. *PLoS Comput. Biol.* **4**, e1000082 (2008).
16. Covert, M.W., Knight, E.M., Reed, J.L., Herrgard, M.J. & Palsson, B.O. Integrating high-throughput and computational data elucidates bacterial networks. *Nature* **429**, 92–96 (2004).
17. Feist, A.M. *et al.* A genome-scale metabolic reconstruction for *Escherichia coli* K-12 MG1655 that accounts for 1260 ORFs and thermodynamic information. *Mol. Syst. Biol.* **3**, 121 (2007).
18. Messner, K.R. & Imlay, J.A. Mechanism of superoxide and hydrogen peroxide formation by fumarate reductase, succinate dehydrogenase, and aspartate oxidase. *J. Biol. Chem.* **277**, 42563–42571 (2002).
19. Edwards, J.S., Ibarra, R.U. & Palsson, B.O. *In silico* predictions of *Escherichia coli* metabolic capabilities are consistent with experimental data. *Nat. Biotechnol.* **19**, 125–130 (2001).
20. Imlay, J.A. Pathways of oxidative damage. *Annu. Rev. Microbiol.* **57**, 395–418 (2003).
21. Winter, J., Ilbert, M., Graf, P.C., Ozcelik, D. & Jakob, U. Bleach activates a redox-regulated chaperone by oxidative protein unfolding. *Cell* **135**, 691–701 (2008).
22. Taber, H.W., Mueller, J.P., Miller, P.F. & Arrow, A.S. Bacterial uptake of aminoglycoside antibiotics. *Microbiol. Rev.* **51**, 439–457 (1987).
23. Jensen, P.R. & Michelsen, O. Carbon and energy metabolism of atp mutants of *Escherichia coli*. *J. Bacteriol.* **174**, 7635–7641 (1992).
24. Boshoff, H.I. *et al.* The transcriptional responses of Mycobacterium tuberculosis to inhibitors of metabolism: novel insights into drug mechanisms of action. *J. Biol. Chem.* **279**, 40174–40184 (2004).
25. AbuOun, M. *et al.* Genome scale reconstruction of a Salmonella metabolic model: comparison of similarity and differences with a commensal *Escherichia coli* strain. *J. Biol. Chem.* **284**, 29480–29488 (2009).
26. Becker, S.A. & Palsson, B.O. Genome-scale reconstruction of the metabolic network in Staphylococcus aureus N315: an initial draft to the two-dimensional annotation. *BMC Microbiol.* **5**, 8 (2005).
27. Jamshidi, N. & Palsson, B.O. Investigating the metabolic capabilities of Mycobacterium tuberculosis H37Rv using the in silico strain iNJ661 and proposing alternative drug targets. *BMC Syst. Biol.* **1**, 26 (2007).
28. Schilling, C.H. & Palsson, B.O. Assessment of the metabolic capabilities of Haemophilus influenzae Rd through a genome-scale pathway analysis. *J. Theor. Biol.* **203**, 249–283 (2000).
29. Henry, C.S. *et al.* High-throughput generation, optimization and analysis of genome-scale metabolic models. *Nat. Biotechnol.* **28**, 977–982 (2010).

ONLINE METHODS

Antibiotics and chemicals. All chemicals and antibiotics were purchased from Sigma or Fisher Scientific. Concentrated stock solutions of menadione, H_2O_2, NaOCl and all antibiotics were prepared fresh daily. H_2O_2, NaOCl, ampicillin and gentamicin were diluted with or dissolved in sterile deionized water. Ofloxacin and ciprofloxacin were dissolved in 0.1 N NaOH. Tetracycline was dissolved in 50% ethanol (v/v). Menadione, carboxin and chloramphenicol were dissolved in 100% ethanol.

Strains and media. *E. coli* MG1655 was used in this study. Genetic deletions of *aceA*, *appB*, *atpC*, *cyoA*, *edd*, *fumB*, *fbaB*, *gdhA*, *gltB*, *gnd*, *mqo*, *nuoG*, *pfkB*, *pta*, *pykA*, *rpiB*, *sdhC*, *sucC*, *talB*, *tktB* and *zwf* were transduced from the Keio single-gene deletion knockout library[30] into MG1655 using the P1 phage method, and confirmed with PCR. The medium used for all experiments was M9 minimal media with 10 mM glucose as the sole carbon source or MOPS minimal media with 10 mM glucose (for the HyPer protein experiments).

Plasmids. The O_2^- response sensor used in this study was constructed previously[7], and used the native *soxS* promoter upstream of the *gfpmut2* gene. The H_2O_2 response sensor used the same plasmid backbone and was constructed by PCR-amplifying the native *dps* promoter and cloning it into the BamHI and XhoI restriction sites, which formerly contained the *soxS* promoter. The forward primer for PCR was GCGCCTCGAGCCGCTTCAATGGGGTCTA CGCT and the reverse primer was GGCCGGATCCTCGGAGACATCGTTG CGGGTAT. The H_2O_2 response sensor was confirmed to increase expression of GFP upon addition of H_2O_2.

GFP reporter assays. Fluorescent measurements were done on a SpectraMax M5 plate reader (Molecular Devices) using Costar black, clear, flat bottom 96-well plates (Fisher). Each well contained 195 µL of M9 minimal glucose media with ampicillin (100 µg/mL) and 5 µL of overnight culture (plasmids carry an AmpR gene for selection). Overnight cultures were grown in M9 minimal glucose media. Strains were grown in the plate reader at 37 °C with shaking. OD_{600} and fluorescence (excitation: 488 nm, emission: 520 nm, bottom read) were monitored every 10 min. Fluorescence/A_{600} values were calculated using ordinary least-squares regression for measurements between $A_{600} = 0.1$ and $A_{600} = 0.4$. [Yes]Values reported in **Supplementary Table 5** are the relative mean and standard error mean for at least three independent biological replicates. *P* values were calculated using a single-tailed, two-sample *t*-test, assuming unequal variance.

HyPer assays. The HyPer protein is a fluorescent probe that was made by inserting a circularly permuted yellow fluorescent protein into the H_2O_2-sensitive regulatory domain of OxyR[31]. In the presence of increasing concentrations of H_2O_2, the probe's excitation peak shifts ratiometrically from 420 nm to 500 nm, which allows for quantitative measurement of cellular H_2O_2 levels[31,32]. HyPer is based on an *E. coli* H_2O_2-sensing domain, and has been shown to be effective at sensing H_2O_2 within *E. coli*[31]. HyPer was provided from the manufacturer (Evrogen) as an IPTG-inducible gene in a pQE30 vector (ampicillin selection marker)[31]. Single colonies of strains were inoculated into LB media supplemented with 50 µg/mL ampicillin and grown overnight at 37 °C. The *ΔatpC* and *Δzwf* strains were run separately with wild type because those strains grew significantly slower than the other mutant strains. Strains were inoculated 1:100 into MOPS minimal media plus 10 mM glucose and 50 µg/mL ampicillin, and grown to an A_{600} of 0.2–0.3. All cultures were then diluted with MOPS minimal media plus 50 µg/mL ampicillin in a black, clear-bottom 96-well plate to a final A_{600} of 0.05, in a final volume of 200 µL per well. 20 µL of mineral oil (Sigma-Aldrich) was added to each well to prevent evaporation. Strains were grown with and without 75 µM IPTG in a SpectraMax M5 plate reader (Molecular Devices) at 37 °C with shaking, and A_{600} and fluorescence (excitation: 420 nm and 500 nm, emission: 530 nm, bottom read) were monitored every 15 min for 12 h. Measurements between $A_{600} = 0.2$ and $A_{600} = 0.6$ were corrected for background strain fluorescence by subtracting the fluorescence values for uninduced cultures at the same cell density, as measured by A_{600}. The 420 nm × 500 nm curve was linear over this region, and therefore ordinary least-squares regression was used to interpolate between time points. The 500 nm excitation fluorescence value that corresponded with 55 fluorescence units from 420 nm excitation was calculated and the 500/420 ratio was obtained for all strains. Values reported in **Supplementary Table 6** are the relative mean and standard error mean for three independent biological replicates. *P* values were calculated using a single-tailed, two-sample *t*-test, assuming unequal variance.

Antimicrobial sensitivity assays. Strains were grown aerobically from an initial inoculation of $A_{600} = 0.01$ to $A_{600} = 0.16$–0.20 in 250 mL baffled flasks filled to 1/10th the total volume and shaken at 300 r.p.m. at 37 °C. For menadione, H_2O_2 and antibiotic sensitivity assays, time-zero samples were collected (200–400 µL), then 1 mL aliquots were transferred to 14 mL test tubes, and appropriate volumes of menadione, H_2O_2 or antibiotic stock solutions, not in excess of 15 µL, were added to obtain the final concentrations (1 mM menadione, 5 mM H_2O_2, 7.5 µg/mL ampicillin, 100 ng/mL ofloxacin, 15 ng/mL ciprofloxacin, 500 ng/mL gentamicin, 10 µg/mL tetracycline and 15 µg/mL chloramphenicol). For NaOCl, due to its reactivity with media components[33], 10 mL of culture was centrifuged at 3,000 r.p.m. for 10 min in a benchtop centrifuge, 9.5 mL of the supernatant was removed and the cell pellet was resuspended with 9.5 mL of sterile PBS at pH 7.2. The suspension was spun down again at 3,000 r.p.m. for 10 min, and 9.5 mL of the supernatant removed. The cell pellet was resuspended with 4.5 mL of sterile PBS. The cell density was adjusted with sterile PBS to achieve an $A_{600} = 0.2$. Time-zero samples were collected (200–400 µL), 1-mL aliquots were transferred to 14-mL test tubes and NaOCl stock solution was added to obtain the final concentration (20 µM NaOCl). At the specified times (1, 2 h for menadione, H_2O_2, NaOCl; 1, 2, 3, 4 h for antibiotics), sample aliquots were collected (200–400 µL). All samples were immediately centrifuged at 10 k r.p.m. in a microcentrifuge, 95% of the supernatant was removed and the cell pellets were resuspended in PBS. Samples were serially diluted and plated on LB agar plates, which were then incubated overnight at 37 °C. Colony forming units were counted approximately 16-18 h after plating.

Carboxin inhibitor experiments. Strains were grown aerobically from an initial inoculation of $A_{600} = 0.01$ to $A_{600} = 0.16$–0.20 in 250-mL baffled flasks filled to 1/10th the total volume and shaken at 300 r.p.m. at 37 °C. Time-zero samples were collected (200–400 µL), then 1 mL aliquots were transferred to 14-mL test tubes. Carboxin solubilized in 100% ethanol or ethanol alone was added to the tubes. Carboxin was added at a final concentration of 500 µM. H_2O_2 or ampicillin stock solutions were added to obtain the final concentrations of 5 mM H_2O_2 and 10 µg/mL ampicillin. A dose response was also performed of both carboxin (0, 250, 500, 750 and 1,000 µM) and ampicillin (0, 5, 7.5, 10 and 15 µg/mL) to determine if the two compounds demonstrate a synergistic interaction. Drug synergism was calculated using the Bliss Independence and Highest Single Agent models[34,35]. Specifically, the formula, $BIC_{AB} = A + B - AB$ (1), was used to calculate synergism with the Bliss Independence model. A and B are the effects of the two drugs in isolation, whereas, BIC_{AB} is the combined effect of the two drugs as predicted by the Bliss Independence model. If C_{AB}, the experimentally determined combined effect of the two drugs, is $>BIC_{AB}$, synergy is observed. In contrast, in the Highest Single Agent model, if $C_{AB} > \max(A, B)$, synergy is observed. As we were monitoring cell death, the quantitative effect of each compound was defined as the fractional reduction of the population, $R = 1 - CFU_t/CFU_0$, where CFU_t is the number of CFUs measured after treatment, and CFU_0 is the number of CFUs measured before treatment. R = 1 indicates complete loss of the population, R = 0 indicates a population in stasis and R < 0 indicates a growing population. As carboxin was non-lethal and allowed significant growth, even at concentrations as high as 1 mM, the Highest Single Agent model was a much more stringent measure of synergy than the Bliss Independence model. To prove this, let us rewrite the Bliss Independence model as follows: $BIC_{AB} = A(1 - B) + B$ (2). If A is a compound that reduces CFUs, such as ampicillin, its effect above the MIC will be $0 \le A \le 1$, whereas if B is a compound that allows growth at all concentrations, its effect will be $B < 0$ regardless of the concentration. Rearrangement of the above yields $BIC_{AB}/A = 1-B + B/A$ (3). As equation (3) yields $BIC_{AB}/A < 1$ for all $B < 0$ and $0 < A < 1$, the Highest Single Agent model requires $C_{AB}/A > 1$ and the Bliss Independence model requires $C_{AB}/BIC_{AB} > 1$ for synergy, the Highest Single Agent model will always be a more strict synergy requirement under these conditions. Synergy can readily be observed from

doi:10.1038/nbt.2458

the relative survival curves in **Supplementary Figure 4** (curves substantially lower than 1) where 7.5 and 10 μg/mL ampicillin synergize with carboxin concentrations from 250–1,000 μM.

Modeling *E. coli* ROS metabolism. Systems-level metabolic modeling was performed using flux balance analysis and the COBRA Toolbox[36]. Aerobic *E. coli* metabolism (O_2 uptake = −18.5 mmol/gDW/h[17]) was modeled using iAF1260 with glucose (glucose uptake = −11 mmol/gDW/h[17]) and ammonia as the sole carbon and nitrogen sources. The model was augmented with ROS-generating reactions as described in the **Supplementary Methods**. Single-gene deletion analysis was done using the built-in COBRA function. Complete modeling details are provided in the **Supplementary Methods**.

Statistical analysis of model performance. Statistical significance was assessed using the null hypothesis that random selection of genes would match experimental results as well as predictions from our modeling approach. For the GFP reporter systems, where N genes exhibited an increased ROS/BM compared to wild type ($P < 0.05$), and M genes did not ($N + M$: total number of genes tested), we identified the number of genes, P, our approach predicted to increase ROS/BM. We calculated the (a) total number of ways to pick P genes from $N + M$, and then calculated the (b) number of ways to pick P genes that would yield C correct predictions, C being defined as the correctly predicted number of genes our approach identified to increase ROS/BM. The ratio of (b)/(a) is the probability that random selection would yield the same frequency of correct predictions as our approach. Agreement was assessed by calculating the number of predictions that agreed with experimental results. For the O_2^--sensing GFP reporter, 17 of the 21 genes (81%) experimentally tested qualitatively agreed with predictions, whereas for the H_2O_2-sensing GFP reporter, 19 of the 21 genes (90%) experimentally tested qualitatively agreed with predictions. Identical procedures were used in the analysis of HyPer results, except that a P value of 0.1 was used to identify genes that exhibited an increased H_2O_2/BM compared to wild type. For antimicrobial sensitivity assays, statistical significance was assessed similarly, except that N in this case is the number of genes that exhibited a twofold increase in susceptibility toward any oxidant after a treatment time of 2 h.

30. Baba, T. *et al.* Construction of *Escherichia coli* K-12 in-frame, single-gene knockout mutants: the Keio collection. *Mol. Syst. Biol.* **2**, 2006.0008 (2006).
31. Belousov, V.V. *et al.* Genetically encoded fluorescent indicator for intracellular hydrogen peroxide. *Nat. Methods* **3**, 281–286 (2006).
32. Malinouski, M., Zhou, Y., Belousov, V.V., Hatfield, D.L. & Gladyshev, V.N. Hydrogen peroxide probes directed to different cellular compartments. *PLoS ONE* **6**, e14564 (2011).
33. Dukan, S. & Touati, D. Hypochlorous acid stress in *Escherichia coli*: resistance, DNA damage, and comparison with hydrogen peroxide stress. *J. Bacteriol.* **178**, 6145–6150 (1996).
34. Yeh, P. & Kishony, R. Networks from drug-drug surfaces. *Mol. Syst. Biol.* **3**, 85 (2007).
35. Hegreness, M., Shoresh, N., Damian, D., Hartl, D. & Kishony, R. Accelerated evolution of resistance in multidrug environments. *Proc. Natl. Acad. Sci. USA* **105**, 13977–13981 (2008).
36. Becker, S.A. *et al.* Quantitative prediction of cellular metabolism with constraint-based models: the COBRA Toolbox. *Nat. Protoc.* **2**, 727–738 (2007).